Semicond. Sci. Technol. **15** (2000) 840–848. Printed in the UK PII: S0268-1242(00)13161-X

Defect monitoring using scanning photoluminescence spectroscopy in multicrystalline silicon wafers

S Ostapenko†, I Tarasov†, J P Kalejs‡, C Haessler§ and E-U Reisner§

† University of South Florida, Center for Microelectronics Research, Tampa, FL 33620, USA
‡ ASE Americas, Billerica, MA, 01821, USA
§ Bayer AG, 47812, Krefeld, Germany

Received 11 April 2000, accepted for publication 2 June 2000

Abstract. Scanning photoluminescence (PL) spectroscopy was performed on as-grown and processed multicrystalline silicon (mc-Si) wafers to investigate the defect distribution affecting the efficiency of solar cells. In highly inhomogeneous mc-Si prepared by (i) edge-defined film-fed growth or (ii) a block-casting technique, regions of a wafer with enhanced recombination activity and reduced minority carrier lifetime exhibit an intensive 'defect' PL band at room temperature with the maximum at about 0.8 eV. By comparing PL mapping with the distribution of dislocations, we present experimental evidence that the 0.8 eV band corresponds to electrically active dislocation networks. This was confirmed using low-temperature PL spectroscopy, which revealed a characteristic quartet of the dislocation D-lines. One of these dislocation lines, D1, can be tracked as temperature increases and linked to the 'defect' band. Strong linear polarization of the 0.8 eV PL band corresponds to a preferential localization of defects in regions with a high level of elastic stress measured with scanning infrared polariscopy. The origin of the 0.8 eV PL band is attributed to dislocations contaminated with impurity precipitates.

1. Introduction

Vigorous growth in the photovoltaic market over the past decade has been predominantly driven by advances in crystalline silicon technology. Multicrystalline silicon (mc-Si), which is produced by many competing techniques, can meet both a low-cost production and a high efficiency requirement for solar cells. It is anticipated that a goal of 18% mc-Si cell efficiency is realistic and achievable. The highest efficiency solar cells require both a high bulk lifetime in the starting material and effective lifetime upgrading during processing into solar cells. An improvement of minority carrier lifetime, or diffusion length, which is used to track recombination properties of silicon wafers, can be readily accomplished through solar cell processing steps such as P diffusion, hydrogenation and Al backside alloying. Since mc-Si wafers are inhomogeneous, lifetime upgrading is not uniform, and areas with initially high and low recombination activity respond differently to a given processing step. This upgrading has been reported in detail for wafers grown by the edge-defined film-fed growth (EFG) technique [1]. For example, as-grown EFG wafer diffusion lengths of 10–100 μm are upgraded to the range of 75–300 μm in a solar cell. The requirement to track such large inhomogeneity has motivated development of mapping techniques with high spatial resolution and high speeds to aid in electronic quality control in manufacturing. Several such techniques in use today include the surface photovoltage (SPV) and photoconductive decay (PCD) methods, which are sensitive to the total number of recombination centres in the bulk and at the surface of a wafer. A new approach to lifetime monitoring is offered by photoluminescence (PL) mapping at room temperature [2, 3]. This can be performed with a high lateral resolution of a few micrometres. An additional advantage of room-temperature PL mapping arises from its spectroscopic capability [4], which allows a selective monitoring of different radiative centres, as reported previously in Czochralski (Cz) silicon [5].

We report here on PL mapping of recombination centres in high-recombination regions of mc-Si wafers. These regions limit solar cell performance, and their monitoring, characterization and reduction is a primary goal in the search for approaches to achieve high cell conversion efficiencies. We present experimental evidence that high-recombination regions are characterized by an intense 'defect' PL band, which we associate with dislocation electrical activity persisting in the solar cell after processing. We compare the as-grown and processed EFG and block-cast mc-Si wafers to show that spectroscopic PL mapping gives a quantitative measurement of the distribution of active dislocations. This allows us to compare and track through solar cell processing the electronic quality of mc-Si wafers grown with different technologies.

0268-1242/00/080840+09$30.00 © 2000 IOP Publishing Ltd

2. Samples and methods

Materials used in this study were square boron-doped mc-Si wafers up to 10×10 cm^2 area and approximately 300 μm thickness prepared with two different growth technologies. One set of samples was produced using a block-casting technique, while the other set was grown with the EFG technique. Some EFG wafers were subjected to solar cell processing steps and tracked with the PL method.

The PL mapping and spectra were analysed using a Spex-500M grating spectrometer coupled to a liquid-nitrogen-cooled Ge detector. The PL signal was processed using a conventional lock-in technique. The PL spectra were corrected to the spectral response of the optical set-up. The 514 nm Ar laser line in a peak power range from 70 to 300 mW was modulated by a mechanical chopper and used as an excitation source. Alternatively, an 800 nm AlGaAs laser diode with 10 nm bandwidth operating in a pulse mode with a peak power up to 140 mW was also used. The spot size of both lasers was approximately 0.5 mm. The absorption coefficients of these laser lines in silicon are 1 μm^{-1} (514 nm) and 12 μm^{-1} (800 nm), which allows modification of the PL excitation depth. PL mapping at room temperature was performed by placing an mc-Si wafer on an X–Z motion stage. Spatial resolution was controlled by the diameter of the laser spot, which ranged from 60 μm up to 1 mm. Temperature studies were carried out from 4.2 to 300 K in a variable-temperature helium cryostat with 1×2 cm^2 samples. The cryostat had an automated temperature control and stabilization capability of 1 °C. For experiments carried out between 300 and 410 K, samples were mounted on a heater in air and the temperature was controlled with a thermocouple.

Infrared polaroid film was used as the linear polarizer to measure PL intensity with polarized light. The film was mounted on a 360° rotary holder and the polarization plane was aligned to specific defects, e.g. EFG crystal grain boundaries, which are easily viewed on the crystal surface. The PL polarization can be noticeably affected by the polarization properties of the spectrometer and optics. To eliminate this instrumental effect, we performed a careful calibration of the optical system using an unpolarized light source consisting of a tungsten lamp and an output optical fibre. To quantify the linear PL polarization signal, one can calculate the degree of polarization using the following relation:

$$P = (I_{\max} - I_{\min})/(I_{\max} + I_{\min}) \times 100\% \qquad (1)$$

where $I_{\max}$ and $I_{\min}$ are two orthogonal polarized PL intensities with maximum and minimum optical output. P is zero for an entirely unpolarized emission and will go up to 100% in absolute value with a completely linearly polarized light signal.

To correlate the PL map with the distribution of extended crystal defects, we scan the dislocation density. Experimentally, structural crystal defects, such as dislocations, can be monitored by counting μm-size etch pits after appropriate chemical etching steps (e.g. a Secco etching). We used a measurement system capable of etch pit density mappings over wafer areas up to 10×10 cm^2. The system consists of a microscope with computer-controlled automatic focusing moving table, and an image analysis software program. Alternatively, a mapping of the dislocation density in mc-Si wafers was performed using a PVScan-5000 photovoltaic analyser, which also employs a light scattering method [6].

For scanning measurements of the residual strains, we adopted a linear polariscope technique [7]. In this method, collimated light from a 75 W halogen tungsten lamp was focused down to 60 μm on the sample. The intensity of the optical transmission was measured in a spectral region of a transmission window where Si is transparent, near $\lambda = 1.3$ μm. Additionally, two infrared linear polarizers were used in the transmission experiment. They can be oriented with respect to a pre-selected crystal direction, such as a grain boundary in mc-Si. One of them (polarizer) is located in front of the sample and the second (analyser) immediately behind the sample. In general, the intensity of polarization transmission can be expressed as follows [8]:

$$I = I_o(1 - R^2)[\cos^2\chi - \sin 2(\varphi - \psi) \times \sin 2(\varphi - \psi + \chi)\sin^2\delta/2] \qquad (2)$$

where I_o is the intensity of incident light, R is the reflectivity, ψ is the principal angle which determines the orientation of the stress axis at the plane, χ is the angle between polarizer and analyser and φ is the azimuth angle of the polarizer. The polarization intensity, I, measured at selected orientations of the polarizer and analyser, depends on the optical retardation parameter δ, which in turn is directly related to the value of the residual elastic strain. To derive this relationship, the following algorithm is applied [8]. Two transmitted intensities of the polarized light are measured: one with polarizer and analyser parallel to each other, $I_\parallel = I(\chi = 0)$, and the second when the polarizer is turned at 90° and orthogonal to the analyser, $I_\perp = I(\chi = \pi/2)$. By measuring the angular φ-dependence of the ratio $I_\perp/(I_\parallel + I_\perp)$ one can determine quantitatively both the optical retardation, δ, and the direction of the principal stress angle, ψ, using the equation

$$I_\perp/(I_\parallel + I_\perp) = \sin^2(\varphi - \psi)\sin^2\delta/2. \qquad (3)$$

As the last step of the analysis, two strain components, $|e_{zz} - e_{xx}|$ and $|e_{xz}|$, can be calculated. The first term represents a difference in tensile strains along crystallographic Z and X directions, while the second term is the shear strain component between Z and X. The following can be used for calculating strains [8]:

$$|e_{zz} - e_{xx}| = (\lambda/\pi d n_o^3)[\delta/(p_{11} - p_{12})]\cos(2\psi) \qquad (4a)$$

$$|e_{xz}| = (\lambda/\pi d n_o^3)(\delta/p_{44})\sin(2\psi) \qquad (4b)$$

where p_{ij} are photoelastic constants, d is sample thickness and n_o is the refractive index of the unstrained material. In our strain study of mc-Si wafers, the following values were used: $\lambda = 1.3$ μm, $n_o = 3.5$, $d = 300$ μm, $p_{11} = 0.081$, $p_{12} = 0.001$, $p_{44} = 0.075$ [9].

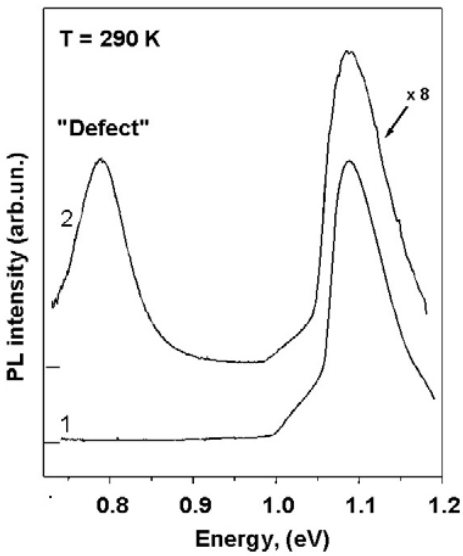

Figure 1. Room-temperature PL spectra in the area with high (1) and low (2) minority carrier lifetime. The 'defect' PL band at about 0.8 eV is observed only in low-lifetime regions of EFG and cast wafers.

3. Experimental results

3.1. Room-temperature PL mapping

The PL spectrum at room temperature is generally composed of two bands in as-grown and processed mc-Si wafers, as shown in figure 1. The high-energy maximum at 1.09 eV corresponds to well known band-to-band emission caused by phonon-assisted recombination of bound and unbound free electrons and free holes [10]. A second broad band at lower energies, with the maximum at about 0.8 eV, is referred to here as the 'defect' band. Both spectral features are very similar in EFG and cast mc-Si. Due to this, the discussion in the following sections applies equally to both materials, unless specifically indicated. We first discuss PL data for the band-to-band PL in conjunction with distribution of minority carrier lifetime.

The recombination rate of minority carriers in Si at room temperature is dominated by non-radiative transitions. It is a basic property of indirect-gap semiconductors, which requires that lattice phonons have to participate in the radiative band-to-band transition in order to have conservation of momentum, and this drastically reduces the probability of such a transition. As a result the PL internal quantum efficiency in Si typically does not exceed 10^{-4} at room temperature [11]. Now the intensity of the band-to-band emission (I_{bb}) in a model neglecting diffusion of carriers can be expressed as follows:

$$I_{bb} \sim \tau_{rad}^{-1}/(\tau_{nr}^{-1} + \tau_{rad}^{-1}) \sim \tau_{nr}/\tau_{rad} \qquad (5)$$

where τ_{rad}^{-1} and τ_{nr}^{-1} are the rates of a radiative band-to-band recombination and non-radiative recombination, respectively, and $\tau_{rad} \gg \tau_{nr}$. The term τ_{nr} thus dominates I_{bb} at room temperature. Generally, the value of τ_{nr} in turn is composed of bulk (τ_b) and surface (τ_s) contributions, and is also known as an effective minority carrier lifetime, τ_{eff}, defined as follows:

$$\tau_{nr}^{-1} = \tau_{eff}^{-1} = (\tau_b^{-1} + \tau_s^{-1}). \qquad (6)$$

Combining equations (5) and (6), one would expect that $I_{bb} \sim \tau_{eff}$. We verified this relation in both EFG and cast mc-Si wafers by performing PL mapping concurrently with the mapping of effective lifetime using a laser-microwave PCD technique. The latter utilizes a high injection rate of minority carriers, matching the PL injection level. Typical results for each material are presented in figures 2(*a*) and (*b*) and 3(*a*) and (*b*). One can clearly observe that the topography of the I_{bb} distribution is very similar to that of the lifetime. We have documented previously that a linear relation between I_{bb} and τ_{eff} is obtained in as-grown cast mc-Si from a point-by-point comparison of maps of both quantities across the wafer [12, 13]. In figure 3, rectangular dark spots in the EFG wafer with reduced I_{bb} and low lifetime are areas with high-recombination due to contacts on the wafer back surface. This confirms that the band-to-band PL is sensitive to recombination lifetime and can be used as a complimentary technique to a lifetime mapping to characterize photovoltaic mc-Si material. We will further demonstrate, below, that scanning room-temperature PL offers opportunities for quality control monitoring in photovoltaic silicon, which extend beyond the standard lifetime mapping techniques.

Inhomogeneity in the electronic properties of both EFG and cast mc-Si wafers gives rise to distinct high- and low-lifetime regions. A low-lifetime region, where the lifetime falls to 50% of its average value in the sample, is framed in figure 2. In the following experiments, we concentrate on examining low-lifetime areas. Besides the low effective lifetime and reduced band-to-band PL intensity, we observe another distinctive feature in the room-temperature PL spectrum in low-lifetime areas. This is an intense PL band with a maximum at about 0.8 eV and a half-width of 72 meV, as shown in figure 1 (curve 2). A typical PL spectrum in a high-lifetime region of mc-Si is also shown in figure 1 (curve 1). We are unable to detect the 0.8 eV band in these high-lifetime areas. The intensity of the defect band, I_{def}, is highly inhomogeneous across the wafer. Even though the PL maximum of the defect band varies between 0.76 and 0.81 eV across the wafer, we can tune the spectrometer to the defect band maximum and scan the wafer to map out the band because the peak shift is typically less than the half-width of the band, and its variation leads to only a small error in I_{def} amplitudes. Using this mapping approach, we observe that the 0.8 eV band is strongly localized in low-lifetime regions, and gives an inverse contrast map to the lifetime and band-to-band PL intensity maps in figures 2(*c*) and 3(*c*). As an example, we indicate by framed areas in these figures the corresponding low-lifetime regions in the wafer. The data confirm that the defect PL band is a reproducible feature of low-lifetime regions in these mc-Si materials, and can be used for identifying low-lifetime regions.

As we reported previously for cast mc-Si, the dislocation density correlates with variations of the defect PL band [12, 13]. We report on a similar study on EFG wafers here. The dislocation density distribution is obtained using a PVScan-5000 system [6]. In figure 4, two line scans across

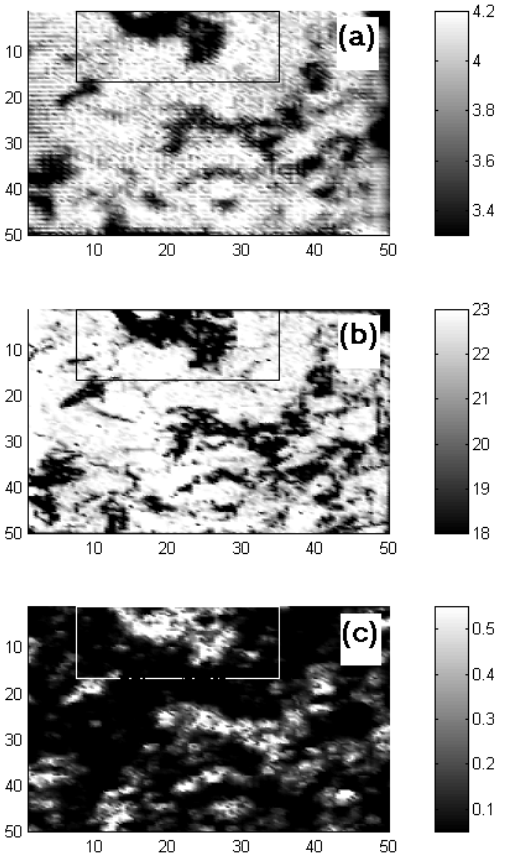

Figure 2. Maps of minority carrier lifetime (*a*), band-to-band PL intensity (*b*) and defect band (*c*) in an as-grown cast mc-Si wafer. The mapped area is 5×5 cm^2. The frame encloses a low-lifetime region.

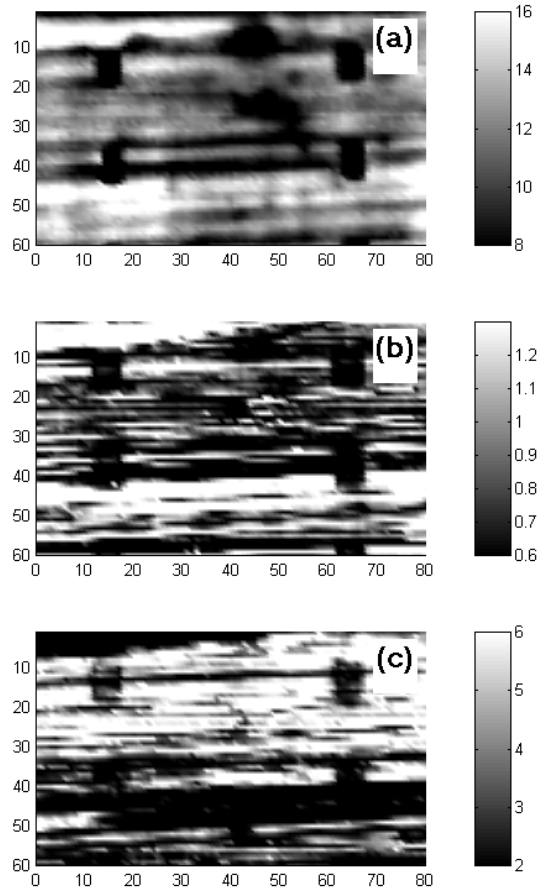

Figure 3. Maps of minority carrier lifetime (*a*), band-to-band PL intensity (*b*) and defect band (*c*) in processed EFG wafers. The mapped area is 8×6 cm^2.

EFG grain boundaries were extracted from full maps, to illustrate the features of the defect PL and dislocation density correlation. The peaks of the ratio $R = I_{\mathrm{def}}/I_{\mathrm{bb}}$, which is proportional to the density of defect centres (see below), coincide with dislocation maxima. The 0.8 eV PL band is observed most consistently in areas with dislocation density $\sim 5 \times 10^6$ cm^{-2}. However, some dislocated areas in the EFG wafer do not show a defect peak. The vertical arrow in figure 4 marks one of these areas. We conclude that, although the defect PL band originates in areas with high recombination activity and increased dislocation density, there are other factors which contribute to produce the defect PL peak. We provide experimental evidence in the next section to help further develop a model of the defect centre that incorporates dislocations.

3.2. Low-temperature PL

We have obtained PL spectra at various temperatures down to 4.2 K in low-lifetime regions with an intense 0.8 eV PL band. The excitation laser was focused to a 1 mm spot. Three PL spectra at different temperatures measured at the same spot on an EFG wafer are compared in figure 5. The defect band is centred on 0.77 eV at 290 K. As the temperature is lowered, both peaks shift to higher energies due to the temperature dependence of the Si bandgap energy. This bandgap increase

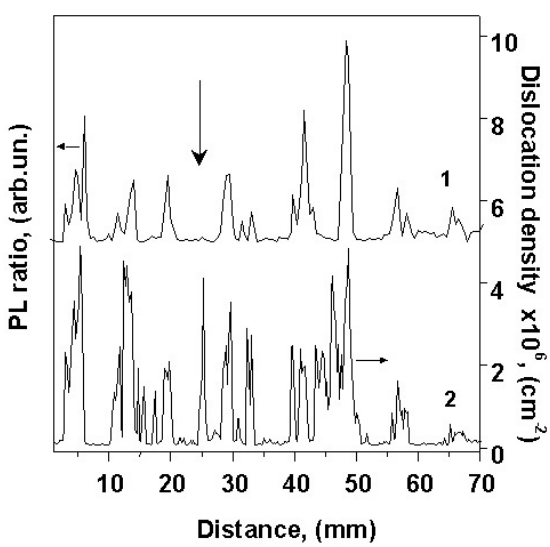

Figure 4. Line scans of the defect concentration expressed as the ratio of defect PL and band-to-band PL (1) and dislocation density (2) in an as-grown EFG wafer. In contrast to a positive correlation of both values, the vertical arrow indicates the region with a high dislocation density and low defect concentration.

between 290 and 77 K is 39.6 meV [10], which is close to the shift of the defect band maximum. At 77 K, rich spectral

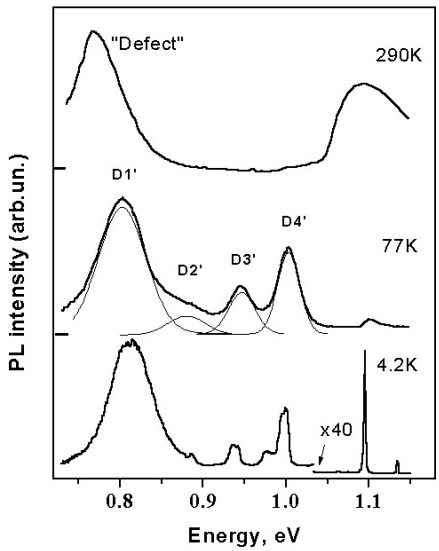

Figure 5. PL spectra of an EFG wafer at different temperatures. The PL spectrum at 77 K is multiplied by four and the room-temperature spectrum by 11. The spectrum at 77 K is deconvoluted numerically to resolve four individual D1′–D4′ Gaussian peaks.

features are now observed at energies below 1.05 eV. Two well resolved new bands appear with maxima at 0.95 and 1.00 eV. At lower energies, the PL spectrum shows the defect maximum near 0.80 eV with a barely resolved additional band as a shoulder. The defect maximum at 290 K thus shifts to higher energies with decreasing temperature, matching the band-to-band temperature shift, and becomes identified with the defect band at 0.8 eV at 77 K. At 4.2 K, the band-to-band emission is replaced by sharp excitonic lines dominated by the TO-phonon replica of the boron bound exciton at 1.093 eV. Along with the increase in intensity between 77 and 4.2 K, the PL bands below 1.05 eV are now much narrower (∼10 meV) and exhibit additional sub-bands. The only exception is the 0.8 eV band, which retains a large half-width of ∼60 meV down to 4.2 K.

We performed a numerical deconvolution of the 77 K PL spectrum in the range of 0.72–1.05 eV, and found that the entire spectrum can be satisfactorily explained by four individual Gaussian bands, D1′–D4′, with peaks corresponding to those of the narrowest lines in figure 5. A set of four PL lines, known as D1–D4, with energies very close to those seen here, was previously observed and studied in detail in plastically deformed Cz and float-zone Si single crystals. These bands are attributed to dislocations [14, 15]. In table 1, we list individual maxima of the four D′-lines in EFG and cast mc-Si wafers, and compare them with the D-lines in Si single crystals. Due to the good correspondence, we assign the four deconvoluted bands in mc-Si, D1′–D4′, in the same sequence as the dislocation lines D1–D4 found in single-crystal silicon. The range of dislocation density measured in low-lifetime regions of our mc-Si wafers (1–8×10^6 cm^{-2}) is at the lower end of the range of dislocation densities reported for the plastically deformed Si exhibiting the dislocation D-lines [14].

Though both quartets of the D-lines are very close as far as their maxima are concerned, there are distinctive features

Table 1. Energy position in eV of D-lines in Si single crystal [13], and corresponding D′-lines in EFG and block-casting mc-Si wafers.

mc-Si (this study)	Si [13]
D1′: 0.80	D1: 0.812
D2′: 0.83–0.89	D2: 0.875
D3′: 0.95	D3: 0.934
D4′: 1.00	D4: 1.000

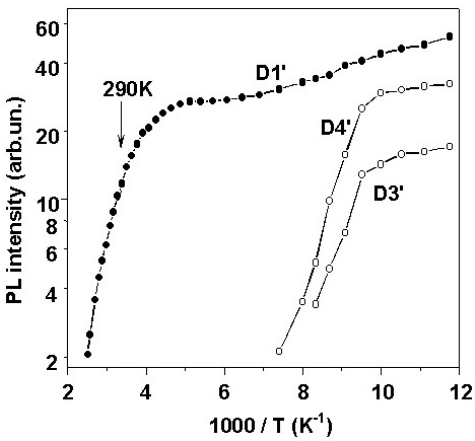

Figure 6. The temperature dependence of the defect PL band (D1′) shows quenching above 200 K with activation energy of 0.26 eV. Temperature quenching of the D3′ and D4′ bands is also depicted.

in the D′-lines in the mc-Si wafers, which distinguish them from single-crystal Si. The most striking are (i) a large half-width for D1′, exceeding its D1 counterpart in crystalline Si by a factor of five, and (ii) a reduced quenching rate at high temperatures for the D1′-line. The latter is illustrated in figure 6. $I_{\rm def}$ starts decreasing only at temperatures above 200 K, with activation energy in the range of 0.24–0.28 eV. This activation energy varies slightly across the wafer. The reduced quenching rate of the DÕ-line, as compared to the D3′ and D4Õ-lines, is primarily responsible for our ability to still see the 0.8 eV band in the room-temperature PL spectrum in mc-Si.

3.3. Polarization study

An interesting property of the 0.8 eV PL band is a linear polarization in optical transitions associated with this band. This is observed in both EFG and cast mc-Si materials. Data illustrating this effect are presented in figure 7 as two PL spectra measured with a linear infrared polarizer oriented in two orthogonal directions of the polarization plane. These two directions were selected at a maximum and minimum of $I_{\rm def}$ versus azimuth angle of the polarizer, as depicted in the inset in figure 7. In contrast to the defect band, the intensity of band-to-band PL measured at exactly the same point on the wafer is unaffected by the polarization direction, i.e. this amplitude is unpolarized. We find in EFG samples that the maximum intensity of the defect PL band is observed when the polarization direction is perpendicular to the nearest grain boundary. We also measured the degree of polarization in other regions of the same EFG wafer, and

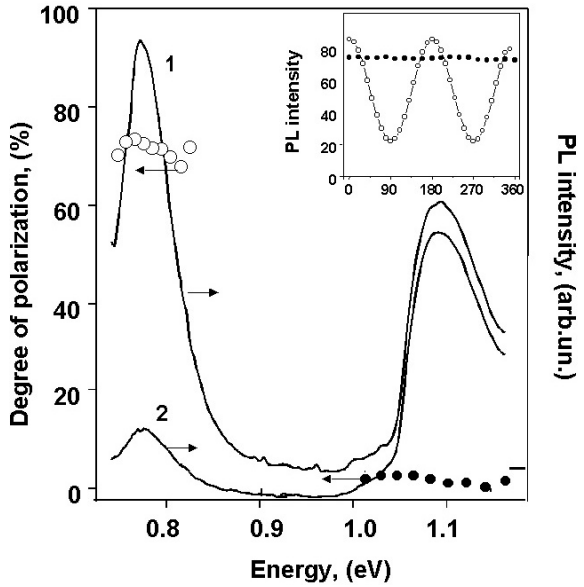

Figure 7. Two PL spectra in an EFG wafer measured in polarized light at orthogonal orientations of the polarizer corresponding to (1) maximum $\chi = 0^\circ$ and (2) minimum $\chi = 90^\circ$ intensity of the defect PL angular dependence as shown in the inset. The spectrum (1) has y-axes offset. Circles represent spectral dependence of the degree of polarization for defect PL (open circles) and band-to-band PL (solid circles). The inset shows the angular dependence of both PL intensities.

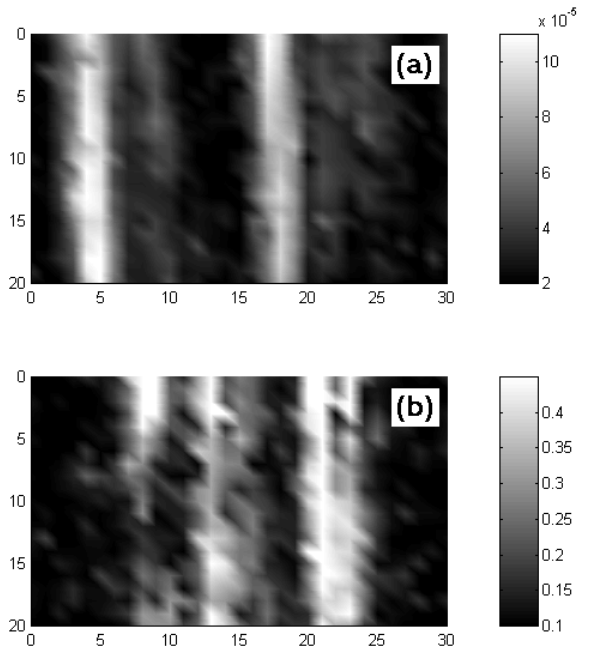

Figure 8. Maps of residual strains (a) and the defect PL band (b) in an as-grown EFG wafer. The mapped area is 20×30 mm^2 using a step of 200 μm. White contrast corresponds to higher PL intensity and higher stress. The maximum stress value in the map is 10 MPa.

found that it varies between 58 and 72%. Similar values of the degree of polarization were found in the cast material. It is important to note that this is a very high degree of polarization, and corresponds to strongly polarized optical transitions, a situation which is only observed in Si single crystals subjected to uniaxial stress [15]. This suggests that the internal stress field due to crystallographic defects—grain boundaries and dislocations—is a source of the anisotropy revealed by this polarization in the PL defect band.

To clarify this situation, we performed a polarization transmission study of the strain distribution in EFG wafers using scanning linear polariscopy. The strain maps were compared with a distribution of the defect PL band intensity on the same wafer using an identical optical alignment. In this experiment, the PL was excited using the 514 nm line of the Ar^+ laser focused down to a 100 μm spot on the frontside of the wafer, and the PL was recorded from the backside of the wafer. This optical alignment allowed correct comparison of PL and strain maps measured with identical high resolution. First, we measured the angular dependence of the ratio $I_\perp/(I_\parallel + I_\perp)$ in the high-strain regions (see equation (3)), and found that the principal angle ψ is close to zero, i.e. the strain axis is aligned within 10° with the nearest grain boundary. This allowed us to limit the strain measurements to mapping of the tensile component, $|e_{zz} - e_{xx}|$, and neglect the complementary component e_{xz} according to equation (4).

A typical result of strain field mapping is presented in figure 8(a) for a 20×30 mm^2 segment of the wafer measured with a 200 μm step. The strain field component, $|e_{zz} - e_{xx}|$, calculated using equation (4a), has a linear geometry and mirrors the orientation of the nearby grain boundary. The maximum value of the strain on this map is 10^{-4}, which corresponds to a stress of 10 MPa in silicon. In mapping the entire 10×10 cm^2 wafer, we found regions with stress as high as 25 MPa. The defect PL band distribution has a distinctive linear distribution of maxima in the vicinity of the high-stress areas, as seen in figure 8(b). The maximum defect peak signals come from regions located on both sides of the stress concentration, in some cases within a few hundred micrometres of the area of maximum stress. It may be significant that the defect PL maxima do not directly coincide with the bands of maximum stress, but are adjacent to these stress areas. The defect centres responsible for the 0.8 eV PL band appear to be strongly affected by the anisotropic stress field of crystallographic defects, which leads to the high degree of polarization observed for this band.

3.4. Solar cell processing

Since the defect 0.8 eV PL band is strongly localized in areas with reduced lifetime in the mc-Si, it can be used to benchmark low-lifetime regions. Moreover, room-temperature PL mapping using different bands in the spectra allows one to selectively assess the concentration of the relevant defects. Their distribution across the as-grown material can be mapped and variations tracked during solar cell processing. The following two-step process will illustrate the approach, which is similar to the doping control in Si using the exciton luminescence [16]. First, we obtain consecutively two PL maps, one for the band-to-band peak and the second for the 'defect' peak, by scanning exactly the same points in the wafer. Next, the concentration of the defect centres and its distribution is deduced from the point-by-point ratio of both intensities by the following analysis. The intensity of both bands, $I_{\rm bb}$ and $I_{\rm def}$, at a constant generation

rate, G, is expressed similarly to equations (5) and (6) as follows:

$$I_{bb} = C_1 \times G \times \tau_{eff}/\tau_{rad} \quad (7)$$

$$I_{def} = C_2 \times G \times \tau_{eff}/\tau_{SRH} \quad (8)$$

where $\tau_{SRH} = (N_{def}\, v_{th}\, \sigma_n)^{-1}$ is the Shockley–Read–Hall radiative lifetime, N_{def} is the concentration of defect centres, v_{th} and σ_n are the electron thermal velocity and capture cross section and C_1 and C_2 are temperature dependent Si constants.

A new parameter, $R = I_{def}/I_{bb}$, is introduced, to measure the point-by-point ratio of the two PL peak amplitudes. It is straightforward from equations (7) and (8) to show that the parameter

$$R = I_{def}/I_{bb} = \text{const} \times N_{def} \quad (9)$$

allows a direct mapping of the defect concentration at a constant excitation intensity. R is independent of other recombination channels in the bulk and at the surface, which contribute to τ_{eff}. This feature is also very beneficial to analyse the defect distribution in samples with different processing history, which typically have different surface recombination velocities. Finally, we notice that by calibrating the R-value to the absolute concentration of dislocations using for instance the light scattering technique, one can accomplish a quantitative defect mapping.

We illustrate in this section application of the spectroscopic PL mapping to analyse lifetime upgrading in mc-Si wafers during solar cell processing. Both I_{bb} and I_{def} intensities were mapped for five as-grown 10×10 cm^2 EFG wafers, and an initial distribution of the R-parameter was obtained as the point-by-point ratio of both intensities for each wafer. Next the wafers were processed with P-diffusion, hydrogenation and backside Al firing using standard cell manufacturing technology, which omitted only the front electrode metallization. The PL band distributions of processed wafers were mapped after each step with exactly the same conditions of optical alignment, and by maintaining constant excitation power. The latter was monitored using the PL intensity from a reference Cz Si wafer placed and maintained in the same X–Z stage all the time. The data from processed wafers were expressed as R-parameter maps and compared to the initial R-maps in the wafers.

Generally, consecutive steps in solar cell processing lead to electronic quality upgrading in EFG mc-Si wafers [1]. This was documented previously as an increase of minority carrier lifetime and the band-to-band PL intensity, as measured by scanning SPV and PL techniques [17]. In the present study, the I_{bb} intensity increased by factors of 27–70 on five measured EFG wafers (table 2). An increase ranging from 15 to 30 was also observed for average I_{def}. The increase of both PL intensities corresponds to upgrading of the effective lifetime according to equations (7) and (8). Our primary concern in this study was monitoring the variation in the R-parameter, which reflects the distribution of the 0.8 eV defect concentration. In figure 9, we present two typical R-maps, initial and processed, for one of the EFG wafers used in this study. Regions of high defect concentration in as-grown wafers are observed after the wafer undergoes the complete cell processing cycle. The average value of the R-parameter

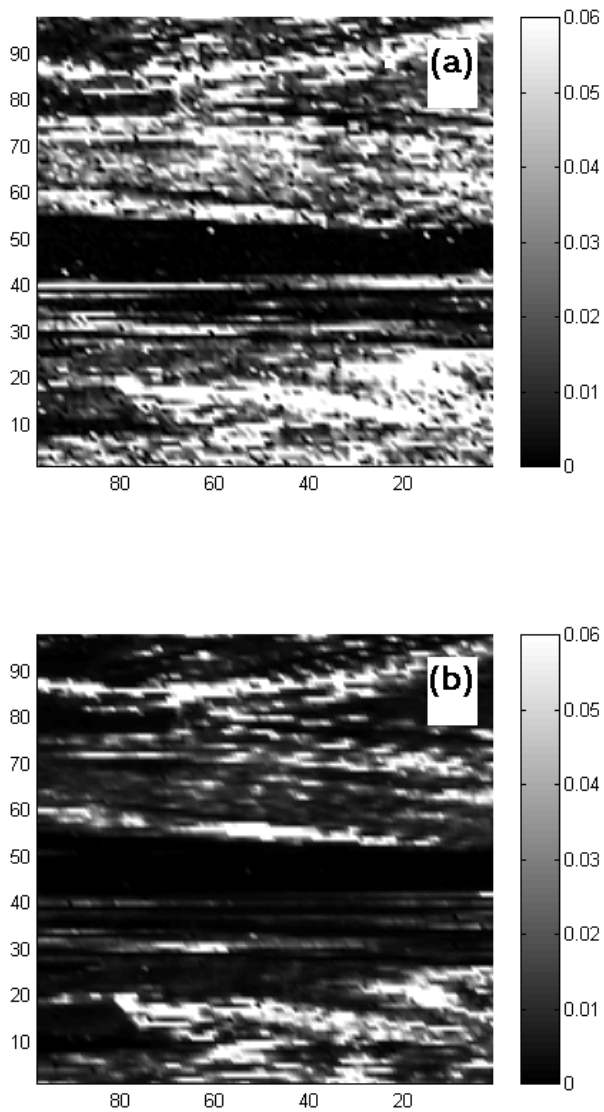

Figure 9. Room-temperature luminescence mapping of the ratio of two PL intensities, $R = I_{def}/I_{bb}$, measured on an entire 100×100 mm^2 area (step size is 1 mm) as-grown EFG wafer (*a*), and the same wafer after solar cell processing (*b*). The average R-value is reduced in the processed wafer by a factor of two (ASE3 in table 2). The front contact grid was not deposited to eliminate blocking of the excitation and luminescence light.

for the wafer is reduced by a factor of two and spans a range of 1.5–3.3 in the five wafers, as compiled in table 2. The factor of two reduction of the defect concentration in wafer no 3 compares to a 70-fold increase of the band-to-band peak intensity. Finally, regions of high defect concentration in processed wafers correspond closely to low-lifetime areas with enhanced minority carrier recombination [18]. This study illustrates how PL spectroscopic maps can be applied in the metrology of the defect concentration in as-grown and processed solar cells.

4. Discussion and conclusions

Low-temperature PL spectroscopy (typically at 4.2 K) is a well known and recognized approach to monitor both doping

Table 2. Change of band-to-band PL (I_{bb}), defect PL (I_{def}) and their ratio (R) averaged across five 10×10 cm^2 EFG wafers after the solar cell processing. The wafer ASE3 corresponds to R-maps in figure 9.

	ASE1	ASE2	ASE3	ASE4	ASE5
I_{bb}(processed)/I_{bb}(as-grown)	55	42	70	27	43
I_{def}(processed)/I_{def}(as-grown)	22	30	25	15	26
R(as-grown)/R(processed)	2.1	1.5	2.0	3.3	2.5

impurities and contamination in Si [19]. For example, it offers a method to make a sensitive quantitative measurement of the concentration of shallow doping centres [16]. There are a few reported cases where room-temperature PL spectroscopy was successfully used in silicon, for instance in monitoring of thermal donors in the annealed Cz Si [20, 21]. Specifically, a band centred at 0.77 eV was observed after two-step annealing and attributed to oxygen precipitates in the vicinity of dislocations. The authors were able to distinguish this band from the dislocation D1-line by a difference in the temperature dependence of the peak amplitude. A broad spectral feature at ∼0.75 eV was observed in the room-temperature PL spectrum of float-zone Si with a dislocation density above 10^8 cm^{-2} introduced by laser melting of the surface [22]. This band was assumed to correspond to the D1 line. These previous PL studies in Si single-crystal materials clearly indicate a dislocation origin for the PL defect band at about 0.8 eV, which agrees with our studies in as-grown and processed mc-Si wafers.

We summarize here the key features of our findings in EFG and cast mc-Si wafers from mapping of the band-to-band (I_{bb}) and defect (I_{def}) PL intensities.

(1) The I_{bb} distribution mirrors that of the effective minority carrier lifetime. This supports the arguments leading to the linear relationship between them, as in equations (5) and (6) above. I_{bb} mapping using a PL spectroscopic technique can identify low-lifetime regions in as-grown mc-Si wafers, and makes possible tracking of their behaviour during solar cell processing of the wafers.

(2) In the regions with reduced I_{bb} and low lifetime, an intense defect band is consistently observed; in contrast, in regions with high lifetime values and reduced total recombination activity, the I_{def} peak is not seen. The topography of the I_{def} map is the inverse of that for lifetime and I_{bb}. One can consider that a direct competition of two radiative channels, the band-to-band and the 'defect' one, can explain the previously observed inverse dependence of I_{bb} and I_{def} [4]. This might occur if the total non-radiative rate is negligible in comparison with radiative rate in low-lifetime regions of the mc-Si. However, our solar cell processing experiments definitely rule this out. In fact, both average intensities, I_{bb} and I_{def}, were noticeably increased after processing (see table 2). According to equations (7) and (8), this requires that the efficiency of other (non-radiative) recombination centres contributing to effective lifetime is reduced. It further implies that the defect band is a signature of a strong non-radiative recombination centre, which exists in as-grown and processed mc-Si, and decreases in concentration during processing from a wafer into a solar cell.

(3) The I_{def} distribution tracks that for dislocations in both cast and EFG mc-Si. The dislocations are an important cause of the current loses in EFG solar cells, as was documented using the temperature dependent EBIC technique [23]. Specifically, a distribution of shallow levels is assigned to the intragranular dislocations. Additionally, low-temperature PL spectroscopy, which shows the link between the dislocation D1-line and the 0.8 eV band, gives clear evidence of the dislocation origin of the defect luminescence. The large half-width of the 0.8 eV band and reduced quenching rate with decreasing temperature in mc-Si, compared to its D1 counterpart in Si single crystals, can be attributed to the result of enhanced interaction of point defects or impurities with dislocations in the case of mc-Si, which modify the recombination parameters of the D1 centres. The influence of oxygen precipitates on the maximum position and on the half-width of the D1-line was previously observed and studied in annealed Cz Si with different initial concentrations of oxygen [24]. The authors interpreted the line half-width increase with oxygen as a strain-induced effect due to oxygen precipitates. Another factor which could modify the D1-line half-width is an interaction of dislocations with heavy metals [25]. In this respect, we point out that heavy-metal precipitates (Fe, Ni, and Cr) have been observed by x-ray fluorescence in low-lifetime regions of both kinds of mc-Si used in our study [26]. We thus propose that impurity precipitates involving oxygen or heavy metals influence the recombination parameters of the D1 centre and create a new channel for non-radiative and radiative minority carrier recombination in mc-Si. The inhomogeneity of precipitates across the wafer can account for the variation of the defect maximum position and half-width found in our study.

(4) A novel property of the defect PL band identified here is the strong linear polarization of the optical transitions. In a highly symmetrical crystal matrix, such as a silicon single crystal with the diamond lattice, the degree of polarization of the PL signal has to be close to zero [27], as we have found for the band-to-band PL intensity. A linear polarization of the PL in cubic crystals can occur due to (i) a local reduction of the crystal field symmetry by an internal stress field and splitting of electronically degenerate levels of a defect or (ii) an optical alignment of corresponding anisotropic defects during cooling in crystal growth resulting from unrelaxed grain-boundary stress. Either of these mechanisms may account for the polarization of the defect band in mc-Si. Tetragonal symmetry in the D1 centre was deduced from uniaxial stress experiments in Si single crystals [15]. The splitting of the D1-line into two polarized components

was found at a [100] orientation of the external stress. In the case of mc-Si, an internal stress can be generated by unrelaxed grain boundaries and dislocations [28]. The internal strain mapping performed in this study with infrared polariscopy shows that defect centres are indeed localized in the vicinity of a high residual strain, which may account for a stress induced polarization of the 0.8 eV band. Finally, the stress effect could be confirmed as a polarization splitting of the band-to-band PL intensity, which was not observed experimentally. The reason is that the pressure coefficient in Si is 4.6×10^{-5} eV MPa^{-1} [29], and even 100 MPa stress would create a splitting of only 4.6 MeV, which is negligible with respect to the 100 MeV half-width of the PL band.

In summarizing the properties of the 0.8 eV defect PL band in mc-Si, we suggest that its luminescence originates from electrically active dislocations, which interact with point defects, impurities or their clusters. It is very likely that oxygen precipitates and heavy metals are mainly involved; however, other impurities such as C and defects formed from self-interstitials or their clusters may also contribute. The defect centres are localized in regions with a high elastic strain field. We have independently assessed the elastic properties of the mc-Si and measured the degree of linear polarization produced by the strain field. Separate mapping of the band-to-band and of the defect luminescence allows for a quantitative measurement of the concentration of the active dislocations in mc-Si. Radiative dislocation centres are modified during solar cell processing, but are still observed in the final device. Additional gettering/passivation is required to completely eliminate these defects and achieve high-efficiency mc-Si solar cells.

Acknowledgments

We would like to thank J Weber for helpful discussions and comments. This work was supported in part by NREL subcontract ACQ-9-29639-03, NSF programme INT-9725215 and ASE Americas.

References

[1] Bailey J, Kalejs J P and Keaveny C 1995 *1st World Conf. on Photovoltaic Energy Conversion* (New York: IEEE) p 1356
[2] Hovel H J 1992 *Semicond. Sci. Technol.* **7** A1
[3] Higgs V, Chin F and Wang X 1998 *Solid State Phenom.* **63/64** 421
[4] Koshka Y, Ostapenko S, Tarasov I, McHugo S and Kalejs J P 1999 *Appl. Phys. Lett.* **74** 1555
[5] Tajima M 1990 *J. Cryst. Growth* **103** 1
[6] Carr K F, Carlson N, Weitzman P, Sopori B L, Marshall C and Allen L 1995 *Defects and Impurity Engineered Semiconductors and Devices* ed S Ashok, J Chevallier, I Akasaki, N M Johnson and B L Sopori (Pittsburg, PA: Materials Research Society) pp 579–83
[7] Lederhandler S R 1959 *J. Appl. Phys.* **30** 1631
[8] Yamada M 1985 *Appl. Phys. Lett.* **47** 365
[9] Shaskolskaia M P (ed) 1982 *Akusticheskie Kristally* (Moscow: Nauka) p 49
[10] Alex V, Finkbeiner S and Weber J 1996 *J. Appl. Phys.* **79** 6943
[11] King O and Hall D G 1994 *Phys. Rev.* B **50** 10 661
[12] Tarasov I, Ostapenko S, Feifer V, McHugo S, Koveshnikov S V, Weber J, Haessler C and Reisner E-U 1999 *Physica* B **273/274** 549
[13] Tarasov I, Ostapenko S, Haessler C and Reisner E-U 2000 *Mater. Sci. Eng.* B **71** 51
[14] Drozdov N A, Patrin A A and Tkachev V D 1976 *JETP Lett.* **23** 598
[15] Sauer R, Weber J, Stolz J, Weber E R, Kusters K-H and Alexander H 1985 *Appl. Phys.* A **36** 1
[16] Tajima M, Masui T, Itoh D and Nishino T 1990 *J. Electrochem. Soc.* **137** 3544
[17] Koshka Y, Ostapenko S, Cao J and Kalejs J P 1997 *26th IEEE PV Specialist Conf. (Anaheim, CA, 1997)* p 115
[18] Tarasov I, Ostapenko S and Kaleis J P *Proceedings of 28th IEEE Photovoltaic Specialists Conference (Anchorage, 2000)* at press
[19] Davies G 1989 *Phys. Rep.* **176** 8
[20] Tajima M, Takeno H, Warashina M and Abe T 1994 *Mater. Sci. Forum* **143–147** 147
[21] Tajima M, Tokita M and Warashina M 1995 *Mater. Sci. Forum* **196–201** 1749
[22] Sveinbjornsson E O and Weber J 1996 *Appl. Phys. Lett.* **69** 2686
[23] Sawyer W D, Bell R O and Sconecker A 1994 *Solid State Phenom.* **37/38** 3
[24] Bugajski M, Goorsky M and Lagowski J 1991 *Electron Technol.* **24** 85
[25] Lightowlers E C and Higgs V 1993 *Phys. Status Solidi* a **138** 665
[26] McHugo S A, Hieslmair H, Weber E R, Rosenblum M D and Kalejs J P 1997 *Defects in Electronics Materials* ed J Michel, T Kennedy, K Wada and K Thonke (Pittsburg, PA: Materials Research Society) p 261
[27] Feofilov P P 1961 *The Physical Basis of Polarized Emission* (New York: Consultants Bureau) p 247
[28] Kwon Y, Danyluk S, Bucciarelli L and Kalejs J P 1987 *J. Cryst. Growth* **82** 221
[29] Smith R A 1964 *Semiconductors* (Cambridge: Cambridge University Press) p 368